Title

Mapping cortical gray matter asymmetry patterns in adolescents with heavy prenatal alcohol exposure.

Journal

NeuroImage, 17(4)

ISSN

1053-8119

Authors

Sowell, Elizabeth R
Thompson, Paul M
Peterson, Bradley S
et al.

Publication Date

2002-12-01

DOI

10.1006/nimg.2002.1328

Peer reviewed

NeuroImage **17,** 1807–1819 (2002)
doi:10.1006/nimg.2002.1328

Mapping Cortical Gray Matter Asymmetry Patterns in Adolescents with Heavy Prenatal Alcohol Exposure

Elizabeth R. Sowell,* Paul M. Thompson,* Bradley S. Peterson,† Sarah N. Mattson,‡ Suzanne E. Welcome,* Amy L. Henkenius,* Edward P. Riley,‡ Terry L. Jernigan,§ and Arthur W. Toga*

**Laboratory of Neuro Imaging, Department of Neurology, University of California at Los Angeles, Los Angeles, California 90095; †Department of Psychiatry, Columbia College of Physicians & Surgeons, and the New York State Psychiatric Institute; New York, New York 10032; ‡Center for Behavioral Teratology, San Diego State University, San Diego, California 92120; and §Department of Veterans Affairs Medical Center, Department of Psychiatry, and Department of Radiology, University of California at San Diego School of Medicine, La Jolla, California 92093*

Received March 21, 2002

Here we report on detailed three-dimensional quantitative maps of brain surface and gray matter density asymmetry patterns during normal adolescent development and show how these anatomical features of the brain are disrupted as a result of prenatal exposure to large quantities of alcohol. We studied two independent samples of normally developing children, adolescents, and young adults, totaling 83 subjects from two different research groups, and compared them to 21 individuals with heavy prenatal alcohol exposure. Surface-based image analysis techniques allowed us to match cortical anatomy across subjects and between hemispheres based on manually delineated sulcal landmarks. Quantitative maps of brain surface asymmetry reveal prominent peri-Sylvian hemispheric differences in which the superior temporal and inferior parietal cortices are shifted backward in the left relative to the right hemisphere in both normal and alcohol-exposed subjects. Cortical surface gray matter asymmetry, mapped here in adolescent populations, is most prominent in the posterior inferior temporal lobes (right greater than left), and this effect does not differ between groups of normally developing children, adolescents, or young adults. Alcohol-exposed individuals show a significant reduction in this asymmetry, whether studied with surface-based or more traditional volumetric region of interest analyses. This region of cortex, near the junction of Brodmann's areas 21, 22, and 37, primarily subserves language functions that are known to be impaired on average in the alcohol-exposed subjects. Our findings elucidate regional patterns of brain surface and gray matter asymmetry during normal development and may contribute to a more comprehensive understanding of the neural substrates of cognitive dysfunction after heavy prenatal alcohol exposure.

INTRODUCTION

Little is yet known about brain asymmetry patterns in normal development or how they are altered in neurodevelopmental disorders such as fetal alcohol syndrome (FAS). FAS, a permanent birth defect caused by maternal consumption of large quantities of alcohol during pregnancy, is a leading cause of developmental disabilities. Even the earliest reports of the syndrome documented significant neurodevelopmental abnormalities (Jones and Smith, 1973) of which microcephaly is the most commonly described (Roebuck *et al.,* 1998). Volumetric (Archibald *et al.,* 2001; Mattson *et al.,* 1996b; Swayze *et al.,* 1997), voxel-based (Sowell *et al.,* 2001b), and surface-based (Bookstein *et al.,* 2001; Sowell *et al.,* 2002a) image analyses have been used to study structural abnormalities *in vivo* in the brains of individuals exposed to alcohol prenatally (ALC). Results from these studies show that brain maturation continues to be adversely affected long after prenatal alcohol exposure. For example, we have shown increased gray matter density and decreased white matter density bilaterally in posterior temporal and inferior parietal regions in ALC subjects (Sowell *et al.,* 2001b, 2002a), suggestive of abnormal myelination during adolescence. The left hemisphere seemed to be more affected than the right, leading us to speculate that the ALC subjects may have altered asymmetry in the perisylvian cortex. To our knowledge, however, no quantitative brain imaging studies have examined structural asymmetry in ALC subjects.

In normal individuals, hemispheric asymmetry in the posterior temporal lobes has been observed in the human *postmortem* literature in adults (Geschwind and Levitsky, 1968; Wada *et al.,* 1975) and in infants (Wada *et al.,* 1975; Witelson and Pallie, 1973). The most frequently studied asymmetry in the imaging and *postmortem* literatures has been a left larger than right planum temporale (Galaburda *et al.,* 1978; Geschwind and Levitsky, 1968; Habib *et al.,* 1995; Kulynych *et al.,* 1994; Steinmetz *et al.,* 1991, 1995; Wada *et al.,* 1975). Gray matter density has been shown to be greater in right posterior temporal regions than in left (Watkins *et al.,* 2001). Also in the posterior temporal lobes, the Sylvian fissure tends to extend more posteriorly in the left hemisphere than in the right (Galaburda *et al.,* 1978; Ide *et al.,* 1996) and angles up more dramatically at its posterior end in the right hemisphere than in the left (LeMay and Culebras, 1972). These

1053-8119/02 $35.00

findings have been further confirmed *in vivo* in normal adults (Narr *et al.,* 2001; Sowell *et al.,* 2002b; Thompson *et al.,* 1998) and in normally developing children and adolescents (Blanton *et al.,* 2001; Sowell *et al.,* 2002b) when surface-based image analysis techniques were used to create maps of sulcal patterns.

In the present report, we assessed brain surface and gray matter density asymmetries in normally developing children and adolescents and in children and adolescents prenatally exposed to large quantities of alcohol. We studied two independent samples of normally developing children, adolescents, and young adults, totaling 83 subjects from different geographic regions, using different magnetic resonance image (MRI) acquisition protocols. We used cortical matching techniques that allowed us to assess differences in gray matter density at homologous anatomic points in the left and the right hemispheres in each subject. The methods used in the present report, in which we assess asymmetry in gray matter density, are new and have not been described in our previous report of sulcal pattern asymmetry in normally developing children (Sowell *et al.,* 2002b), in which we mapped only displacement in the location of cerebral sulci between the left and the right hemispheres. In addition to assessing normative gray matter density asymmetry in children and adolescents in the present report, we tested for differences in gray matter asymmetry between the alcohol-exposed and the normal subjects. Given our earlier findings of hemispheric differences in gray matter density abnormalities in the ALC subjects relative to controls (Sowell *et al.,* 2001b, 2002a), we expected that we would see differences between groups in gray matter asymmetry patterns.

METHODS

Subjects

Table 1 shows an age-by-gender breakdown for all subjects in each group.

TABLE 1

Age-by-Gender Breakdown for All Subjects

	ALC		SDC		YC	
Age	M	F	M	F	M	F
7	—	—	—	—	2	2
8	—	1	1	1	5	1
9	1	3	2	1	1	2
10	2	3	—	2	4	3
11	—	1	—	2	3	2
12	1	—	1	1	5	—
13	—	—	—	2	—	—
14	—	1	1	1	1	1
15	2	1	—	1	3	1
16	2	—	2	—	1	2
17	—	—	—	—	—	2
18	—	—	—	—	3	—
19	1	1	—	—	1	—
20	—	—	—	—	1	—
21	—	—	—	—	1	1
22	1	—	—	—	—	5
23	—	—	—	1	3	1
24	—	—	—	—	1	2
25	—	—	2	—	1	—

Note. ALC, prenatal alcohol exposure; SDC, San Diego controls; YC, Yale controls.

ALC Subjects

Twenty-one children, adolescents, and young adults with prenatal alcohol exposure who were between the ages of 8 and 22 years (mean age 13 years, 11 female, 2 left-handed) underwent MRI at the University of California at San Diego (UCSD). All alcohol-exposed children were evaluated by a dysmorphologist, and all of the children and young adults had histories of heavy prenatal alcohol exposure. Results from neuropsychological testing in these subjects are presented elsewhere (Mattson *et al.,* 1996a, 1999; Mattson and Riley, 1999). Fourteen of them had the characteristic facial appearance (Jones and Smith, 1975) that allowed for a diagnosis of FAS (mean age 12.6 years, 8 female, 1 left-handed). Seven other subjects did not have the facial features to warrant a diagnosis of FAS (mean age 13 years, 3 female, 1 left-handed), but were exposed to large quantities of alcohol *in utero* (we have referred to this group as prenatal exposure to alcohol (PEA)). The FAS and PEA groups (i.e., ALC) were combined for the statistical analyses to increase power, given that similar results have been observed for PEA and FAS subjects in earlier studies of brain morphology (Archibald *et al.,* 2001; Sowell *et al.,* 2001a,b). Full-scale IQ scores were similar for both alcohol-exposed groups (FAS mean = 77, standard deviation = 15, range 49 to 92; PEA mean = 86, standard deviation = 14, range 64 to 101). Children in the FAS and PEA groups were born to women known to drink heavily during pregnancy, either in a binge fashion or more regularly. As in most retrospective studies involving FAS and prenatal alcohol exposure, exact amounts and patterns of maternal drinking were typically not available. All children were screened for prenatal exposure through caregiver self-report. Additionally, for children in the alcohol-exposed groups, maternal self-report and medical, social, and/or legal records were reviewed to confirm prenatal alcohol exposure and to rule out heavy use of other drugs.

Controls

A total of 83 normal children, adolescents, and young adults were studied. Twenty-one between 8 and 25 years (mean age 13.5, 12 female, all right-handed) were recruited and studied at UCSD. These child and adolescent subjects were recruited as normal controls for a large, multidisciplinary neurodevelopmental research center or for the Center for Behavioral Teratology, both in San Diego. The young adult subjects were recruited as normal controls for neuropsychiatric studies of adult patient populations. These subjects were thoroughly screened for medical, neurological, and psychiatric disorders and again informed consent was obtained from each subject. These subjects have been studied as controls in our previous reports of brain structural abnormalities in prenatal alcohol exposure (Sowell *et al.,* 2001a,b,

2002a). An additional 62 normal control subjects between 7 and 25 years (mean age 14.9, 26 female, 60 right-handed) were recruited and studied at the Yale Child Study Center as controls for individuals with tic disorders (described in Peterson *et al.,* 2001). All subjects were screened for neurological impairments, psychiatric illness, history of learning disability, or developmental delay. Informed consent was obtained from all subjects.

Imaging Protocol

UCSD

ALC and control subjects were scanned with a 1.5-T superconducting magnet (Signa; General Electric, Milwaukee, WI). The MRI protocol collected was a whole-brain, gradient-echo (SPGR) T_1-weighted series collected in the sagittal plane with TR = 24 ms, TE = 5 ms, NEX = 2, flip angle 45°, field of view 24 cm, 124 slices with section thickness of 1.2 mm, no gaps, with an imaging time of 19 min.

Yale

All subjects were scanned with a single 1.5-T superconducting magnet (Signa; General Electric). The MRI protocol collected was a whole-brain gradient-echo (SPGR) T_1-weighted series collected in the sagittal plane with TR = 24 ms, TE = 5 ms, NEX = 2, flip angle 45°, field of view 30 cm, 124 slices with section thickness of 1.2 mm, no gaps. Note that the main difference between the Yale and the UCSD protocols is in the field of view parameter.

Image Processing

The SPGR MR images from all subjects were processed with the same series of manual and automated procedures, which are described in detail in other reports (Sowell *et al.,* 1999, 2001c; Thompson *et al.,* 2001) and summarized here.

Preprocessing

First, brain image volumes were transformed into ICBM-305 standard space using a 12-parameter linear (with scaling), completely automated image registration algorithm (Woods *et al.,* 1993). A radiofrequency bias field correction algorithm removed intensity drifts due to magnetic field inhomogeneity (Sled *et al.,* 1998). We increased the number of iterations of the bias field corrector to 200 from an average default of approximately 12 iterations to ensure that the maximal amount of signal drift had been removed from the images. Semiautomated tissue segmentation was conducted for each volume data set to classify voxels based on signal values as most representative of gray matter, white matter, or cerebrospinal fluid (CSF). A simple minimum distance classifier was used because it had previously been shown to provide the best results (for this T_1-weighted imaging protocol) in a qualitative comparison of different tissue segmentation algorithms. A detailed discussion of the reliability and validity of the tissue segmentation protocol has been published elsewhere (Sowell *et al.,* 1999).

Each individual's cortical surface was extracted using automated software (MacDonald *et al.,* 1994) that creates a spherical mesh surface that is continuously deformed to fit a cortical surface tissue threshold intensity value (signal value which best differentiates cortical CSF on the outer surface of the brain from the underlying cortical gray matter) from the brain volume aligned in standard ICBM-305 space (Mazziotta *et al.,* 1995). The resulting cortical surfaces are represented as a high-resolution mesh of 131,072 triangulated elements spanning 65,536 surface points.

Anatomical Analyses

Image analysts (A.L.H., S.E.W.) who were blind to subject gender and age digitized 3D models representative of 17 sulci (Sylvian fissure; central, precentral, postcentral, superior temporal sulcus (STS) main body; STS ascending branch; STS posterior branch; primary intermediate sulcus; secondary intermediate sulcus; inferior temporal, superior frontal, inferior frontal, intraparietal, transverse occipital, olfactory, occipitotemporal, and collateral sulci) in each hemisphere on the surface rendering of each subject's brain (shown in Fig. 1). In addition to the major sulci being contoured, a set of six midline landmark curves bordering the longitudinal fissure were outlined in each hemisphere to establish hemispheric gyral limits. Spatially registered gray-scale image volumes in coronal, axial, and sagittal planes were available simultaneously to help disambiguate brain anatomy. We have developed detailed criteria for delineating the cortical lines and for starting and stopping points for each sulcus, using brain surface atlases as references (Duvernoy *et al.,* 1991; Ono *et al.,* 1990). These criteria have been described previously (Sowell *et al.,* 2002b) and complete details of the written anatomical protocol can be obtained from the authors.

Points on the cortical surfaces between and surrounding the sulcal contours drawn on each individual's brain surface were calculated using the averaged sulcal contours as anchors to drive 3D cortical surface mesh models from each subject into correspondence (Thompson *et al.,* 2000, 2001). This allows the creation of average 3D surface models for the ALC and control groups and the creation of group average maps of various features of the brain surface such as local gray matter density. In this averaging process, a cortical model with the average shape for the group is generated, and features from corresponding gyri are averaged together.

Gray Matter Mapping

Because the deformation maps (acquired during cortical surface matching) associate the same cortical anatomy in each subject (based on sulcal contours drawn in each individual), a local measurement of gray matter density (at each point over the surface of the brain) could be made for each subject and averaged across corresponding regions of cortex (Sowell *et al.,* 2001c, 2002b; Thompson *et al.,* 2001). Briefly, a sphere with a radius of 15 mm centered at each cortical surface point was made and referenced to the same spatial location in the gray matter maps for each subject derived earlier in the tissue classification. The proportion of segmented gray matter voxels relative to the total number of

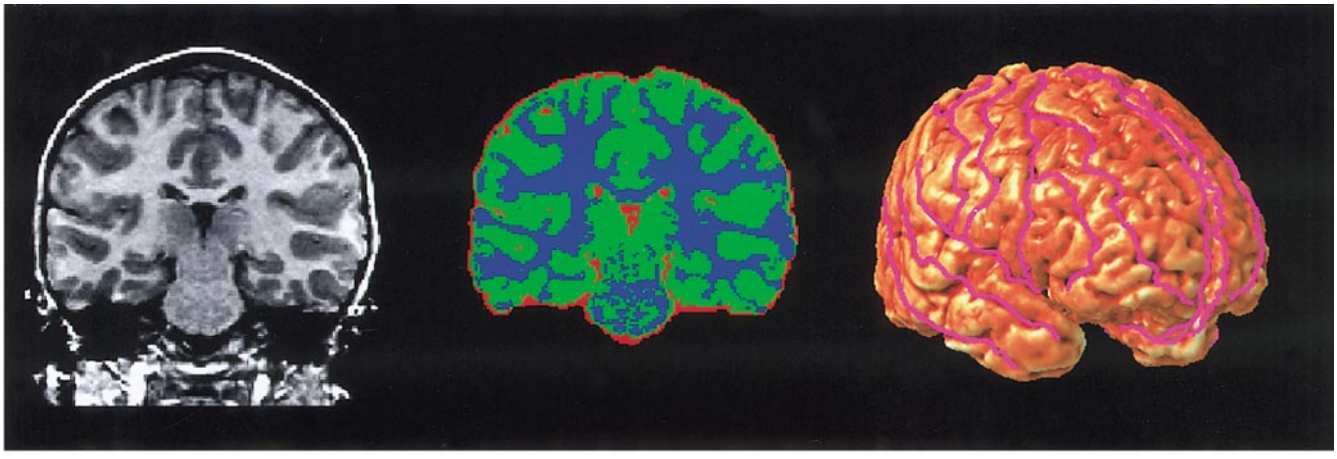

1

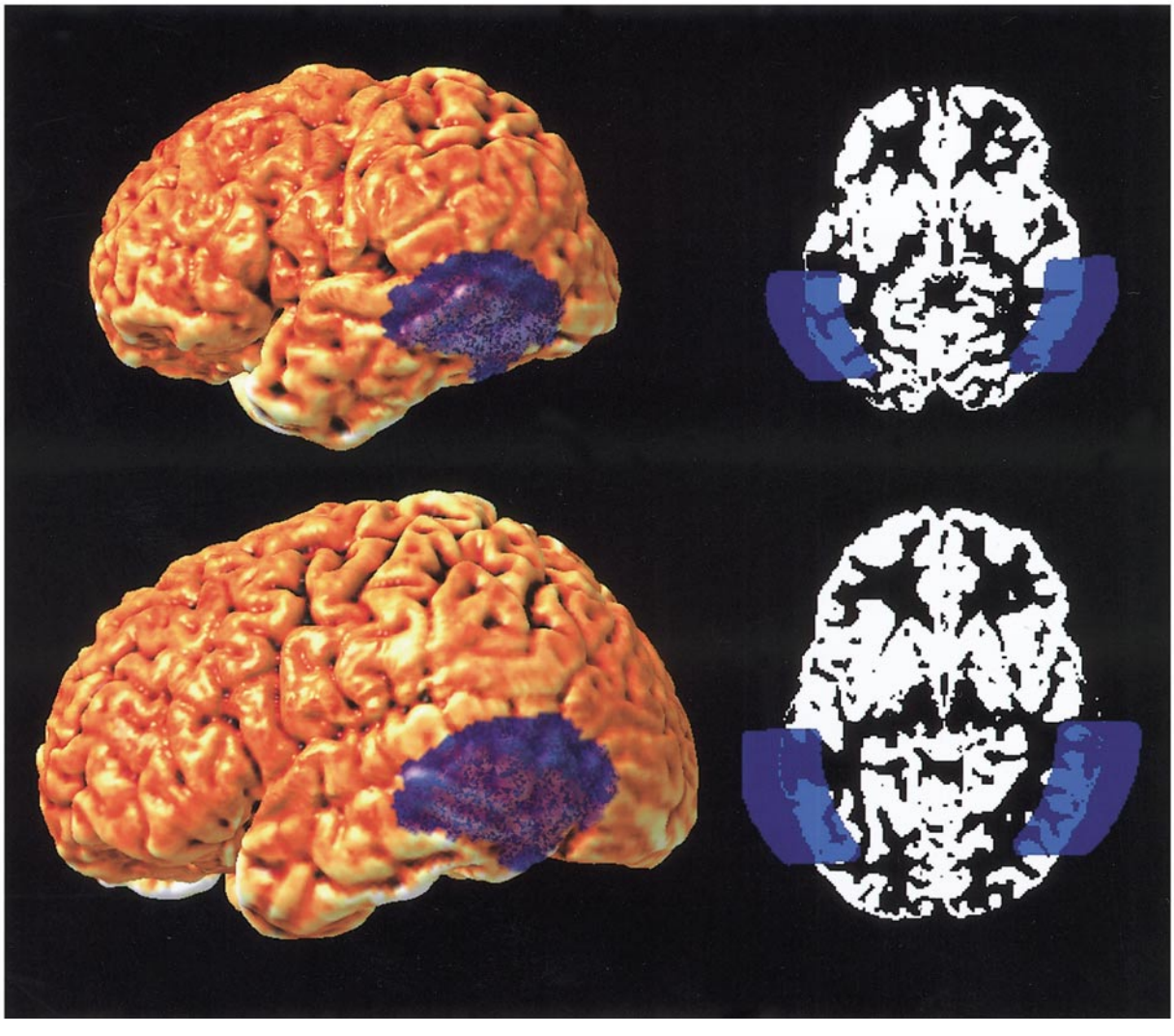

2

FIG. 1. Sample fully processed images. Sample original T_1-weighted (left) and skull-stripped tissue segmented (middle) images and surface rendering (right) with Sylvian fissure; superior and inferior temporal sulci; central, pre-, and postcentral sulci; superior and inferior frontal sulci; and olfactory sulci all drawn in pink. The midline landmark curves bordering the interhemispheric fissure, which are necessary as limiters for the cortical surface matching algorithms, are also shown in pink.

FIG. 2. Statistical region of interest. The ROI (shown in blue) created from the statistical map (shown in Fig. 4) of differences in gray matter density between homologous points in the left and right hemispheres in the SDC group was scaled back into native space and mapped onto the brain surface rendering and gray matter images of two representative individuals. In the top row is one of the smallest brains in the data set from a 9-year-old girl with FAS, and in the bottom row is one of the largest brains in the data set from a normally developing 15-year-old girl. The images also reflect the microcephaly often observed in FAS patients.

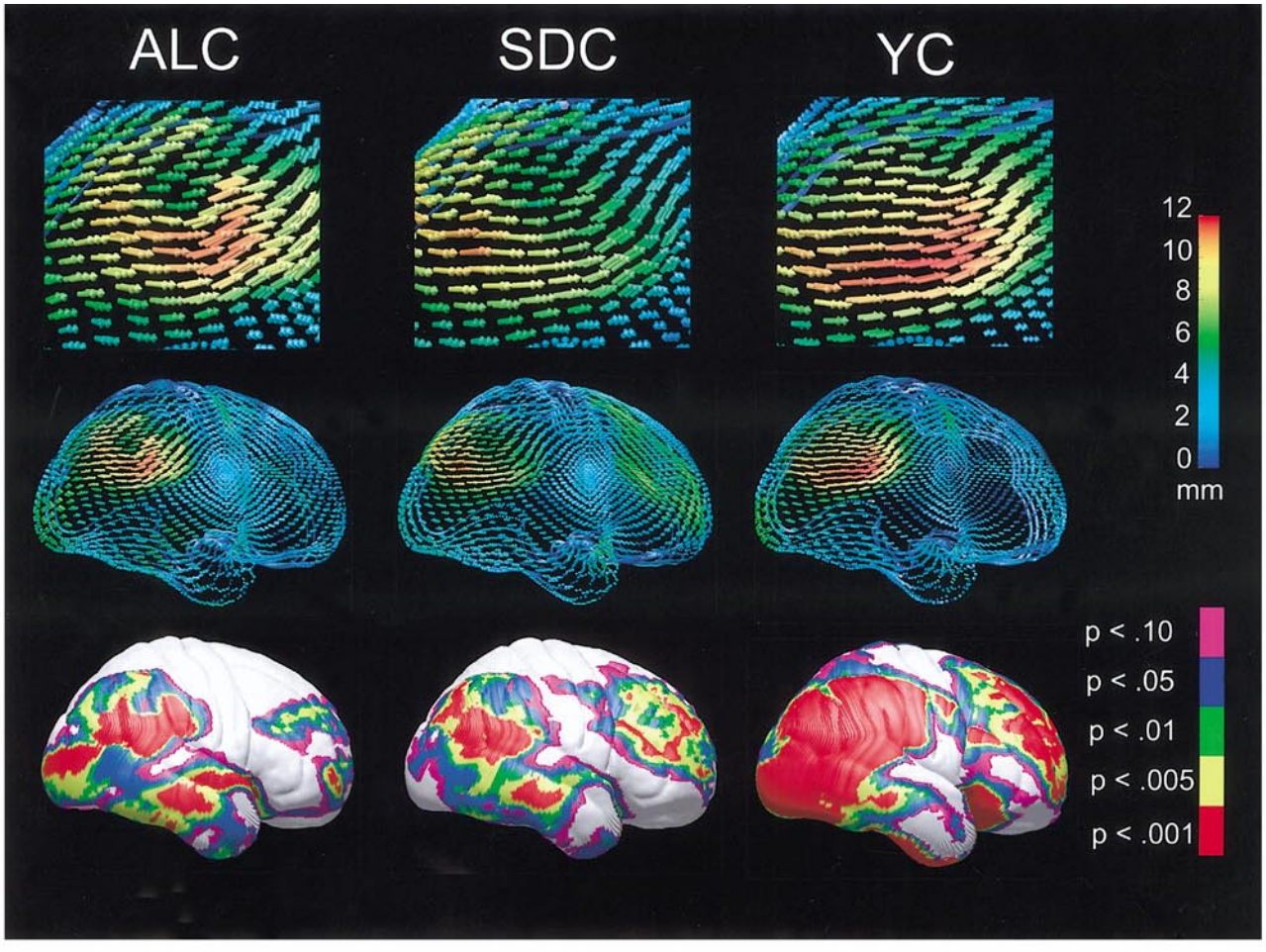
ALC
SDC
YC
12
10
8
6
4
2
0
mm
p < .10
p < .05
p < .01
p < .005
p < .001

3

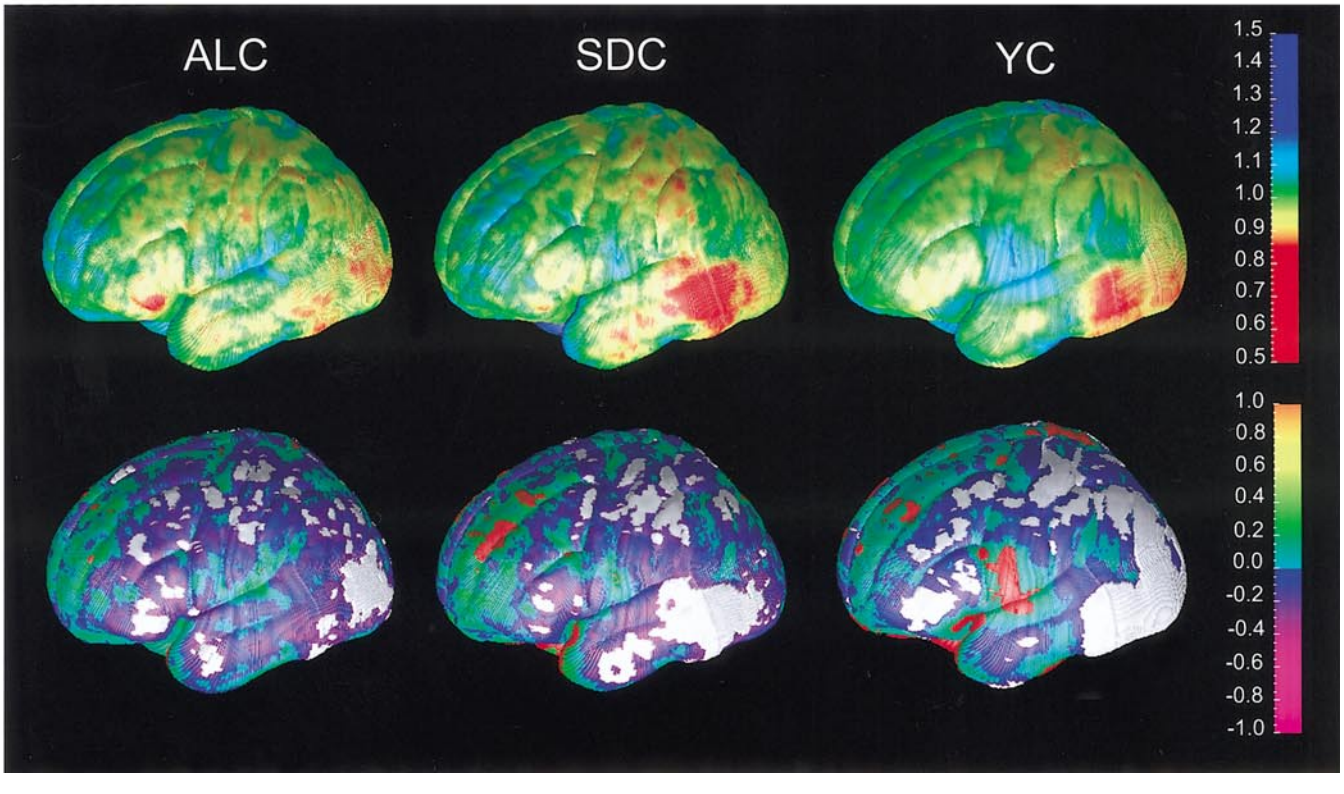
ALC
SDC
YC
1.5
1.4
1.3
1.2
1.1
1.0
0.9
0.8
0.7
0.6
0.5
1.0
0.8
0.6
0.4
0.2
0.0
-0.2
-0.4
-0.6
-0.8
-1.0

4

voxels in this sphere was computed (at each point) and stored as a map of gray matter proportion (with values 0.0 to 1.0), for each subject. The proportion of gray matter in each sphere in each individual is reflective, in part, of local cortical thickness that varies over different regions of the brain.

Mapping Brain Surface and Gray Matter Asymmetry

First, differences in brain surface location between the two hemispheres were computed for each subject by computing a flow of each subject's left hemisphere onto a flipped version of his or her right hemisphere while matching sulcal and gyral patterns. In this way, we could assess the distance in millimeters between analogous anatomical points in the left and the flipped, "sulcally matched" right hemispheres. We then used these flipped sulcally matched brain surface representations to assess ratios of gray matter density at analogous surface points (mapped back to the appropriate locations in the gray matter maps for each individual) in the left and right hemispheres.

Statistical Analyses for Brain Surface and Gray Matter Asymmetry

After the basic preprocessing steps were conducted for each individual, statistical maps were created of differences in surface point location (in the anterior–posterior axis only; *y* coordinate) between the left and the sulcally matched right hemisphere within each group. In these analyses, the correlation (Pearson's *r*) between hemisphere (coded as 0 for left hemisphere and 1 for right hemisphere) and the *y*-coordinate location were assessed at each brain surface point. The difference in *y*-coordinate location between hemispheres at any brain surface point had to reach a threshold of $P = 0.01$ to be considered significant. Similar analyses were conducted to assess for group differences in the distance between *y* coordinates in the left and right hemispheres at each brain surface point. A threshold of $P = 0.05$ was used as a surface point threshold to assess group differences in brain surface asymmetry.

Results for hemispheric differences within groups are reported in terms of "left greater than right," in which the left hemisphere surface point sits at a more posterior *y* coordinate than the right, and "right greater than left," in which the right hemisphere surface point sits at a more posterior *y* coordinate than the left. Note that statistical tests between groups (for surface and gray matter asymmetry) were conducted only for the ALC subjects in comparison with the UCSD controls (SDC), and not the Yale controls (YC), given concerns about pooling data with the slight differences in the image acquisition protocols between the two groups. Gross frontal lobe, parietal lobe, temporal lobe, and occipital lobe anatomical regions of interest (ROI) from a probabilistic atlas (Evans *et al.*, 1996) were used in the permutation analyses to assess regional specificity. The number of surface points within each ROI that were significant at a threshold of $P = 0.01$ were compared to the number of significant surface points within the ROI that occurred by chance when subjects (or hemispheres) were randomly assigned to groups (or sides) in 10,000 new analyses. The permutations allowed us to determine the null distribution to assess the overall statistical significance of our results within the four ROIs. The same ROIs were used in permutation analyses to assess for positive (SDC > ALC) and negative (ALC > SDC) differences between groups in brain surface asymmetry.

Next we used similar methods to assess for differences in gray matter density between the left and the right hemispheres within each group (e.g., ALC, SDC, YC). In these analyses, the correlation (Pearson's *r*) between hemisphere (dummy coded as 0 for left hemisphere and 1 for right hemisphere) and gray matter density was assessed at each brain surface point. The difference in gray matter density between hemispheres at any brain surface point had to reach a

FIG. 3. Brain surface asymmetry maps. The arrows in these maps show the 3D direction and distance of displacement between analogous surface points in the left and right hemispheres for the average ALC, SDC, and YC groups. The base of each arrow represents the left hemisphere surface point location, and the tip of the arrow represents the analogous surface point location in the right hemisphere (a flipped and reflected version). Group differences (in millimeters) are mapped in color according to the color bar on the right. Note that maximal asymmetry, up to 12 mm difference between analogous surface points, is found in the peri-Sylvian region in all three groups, shown enlarged to enhance detail in the top row. Displacement between left and right hemispheres is primarily in the anterior–posterior axis in most regions, more prominent in the peri-Sylvian region. Statistical maps are shown in the bottom row, documenting the significance of displacement between analogous surface points in the left and right hemispheres according to the color bar (note white regions are $P > 0.10$). Note that we have assessed the significance of displacement in only the anterior–posterior direction since that is the primary direction of displacement in the peri-Sylvian region. The probabilities shown are for negative correlation coefficients (left more posterior than right surface point location), as few positive correlation coefficients reached statistical significance and they were all on the inferior surface of the brain not shown here.

FIG. 4. Gray matter density asymmetry maps. In the top row are ratio maps quantifying the amount of gray matter within the 15-mm sphere at each brain surface point in the left hemisphere as a ratio to that of the analogous points in the right hemisphere. One (color coded in green shades) represents complete symmetry. Cooler colors (greater than 1) represent regions where there is more gray matter in the left hemisphere than in the right, and warmer colors (less than 1) represent regions where there is more gray matter in the right hemisphere than in the left. In the bottom row are statistical maps in which shades of green to yellow represent positive Pearson's correlation coefficients (regions where there is more gray matter in the left hemisphere than in the right) and shades of purple and pink represent negative Pearson's correlation coefficients (regions where there is more gray matter in the right hemisphere than in the left) according to the color bar on the right (range of Pearson correlation coefficients from −1 to +1). Regions shown in red correspond to correlation coefficients that show significant increase in gray matter in the left hemisphere relative to the right at a threshold of $P = 0.05$. Regions shown in white correspond to correlation coefficients that show significant increase in gray matter in the right hemisphere relative to the left at a threshold of $P = 0.05$. Note that the pattern is similar in the SDC and YC groups, but the significant regions are much larger in the YC group. This is probably due to the increased power in this sample with nearly triple the number of subjects analyzed in the SDC group.

TABLE 2

Brain Surface Asymmetry Results

	Difference between hemispheres						Difference between groups	
	Left > right			Right > left				
ROI	ALC	SDC	YC	ALC	SDC	YC	ALC > SDC	SDC > ALC
Frontal	**0.012**	**<0.001**	**<0.001**	**0.049**	0.087	**0.030**	0.160	0.287
Occipital	**0.003**	0.061	**<0.001**	1.000	**0.010**	0.231	1.000	**0.006**
Parietal	**<0.001**	**<0.001**	**<0.001**	0.269	0.102	1.000	1.000	0.286
Temporal	**<0.001**	**<0.001**	**<0.001**	1.000	0.288	0.146	0.777	0.508

Note. Permutation analysis results (*P* values) for brain surface asymmetry within groups (difference between hemispheres) and the difference in asymmetry between the ALC and the SDC groups. Left greater than right indicates that surface points sit more posteriorly in the left hemisphere than in the right, and right greater than left indicates that surface points sit more posteriorly in the right hemisphere than in the left. A surface point threshold of $P = 0.01$ was used for all hemisphere difference permutation analyses and a surface point threshold of $P = 0.05$ was used for the group difference permutation analyses. This type of analysis compares the number of surface points within each region of interest (ROI) that differ between groups (or hemispheres) at a particular surface point threshold in the real group (or hemisphere) test and the number of surface points that reach that level of significance by chance when subjects (or hemispheres) are randomly assigned to groups. Significant effects ($P < 0.05$) are shown in boldface.

threshold of $P = 0.05$ to be considered significant. Similar analyses were conducted to assess for group differences in the ratio of left to right gray matter density proportion at each brain surface point. Again, $P = 0.05$ was used as a surface point threshold to assess group differences in gray matter asymmetry. Permutation tests (same as described above for surface asymmetry) were conducted to assess the significance of the statistical maps (left–right gray matter differences within groups and differences in the left–right gray matter asymmetry ratio between groups) and to correct for multiple comparisons.

Image and Statistical Analyses for *post Hoc* Volumetric Measures

Finally, in order to validate observations in the gray matter asymmetry statistical maps, post hoc volumetric analyses were conducted to assess group differences in gray matter *volume* asymmetry in the same regions where group differences in gray matter *density* asymmetry were observed. One new temporal lobe region of interest was automatically defined for each hemisphere in the gray matter image data sets for each individual, based on the statistical maps of differences in gray matter density between the left and the right hemisphere in the SDC group. The ROI was created by selecting all surface points at which the hemispheric difference in gray matter density within the SDC group was significant at a probability of 0.01 or less. Note that a single large cluster of significant surface points within the posterior temporal lobe was targeted given our *a priori* hypotheses regarding peri-Sylvian cortices. The single-voxel layer of surface points (since we measured statistics only at the cortical surface) comprising the new ROI was then dilated (in the left–right direction only) with a 15-mm radius (to emulate the 15-mm radius sphere in the surface-based gray matter density analyses). The new statistical ROI encompassed all voxels which showed a statistically significant difference in gray matter density between hemispheres (within the posterior temporal lobe cluster) and which were within a 15-mm radius of the brain surface. While the ROI reflected differences between hemispheres and was constructed, arbitrarily, in the left hemisphere, we created a flipped version of the same ROI in the right hemisphere for volumetric assessment of gray mat-

TABLE 3

Gray Matter Density Permutation Results

	Difference between hemispheres						Difference between groups	
	Left > right			Right > left				
ROI	ALC	SDC	YC	ALC	SDC	YC	ALC > SDC	SDC > ALC
Frontal	0.952	0.330	0.073	0.097	0.161	0.078	0.316	0.601
Occipital	0.512	1.000	0.312	**0.001**	**0.015**	**0.000**	0.117	0.434
Parietal	0.591	0.571	0.305	**0.037**	**0.017**	**0.012**	0.348	0.221
Temporal	**0.043**	**0.003**	**0.006**	0.155	**0.008**	**0.023**	0.147	**0.049**

Note. Permutation analysis results (*P* values) for gray matter density asymmetry within groups (difference between hemispheres) and the difference in asymmetry between the ALC and the SDC groups. A surface point threshold of $P = 0.05$ was used for all hemisphere and group difference permutation analyses. Significant effects ($P < 0.05$) are shown in boldface.

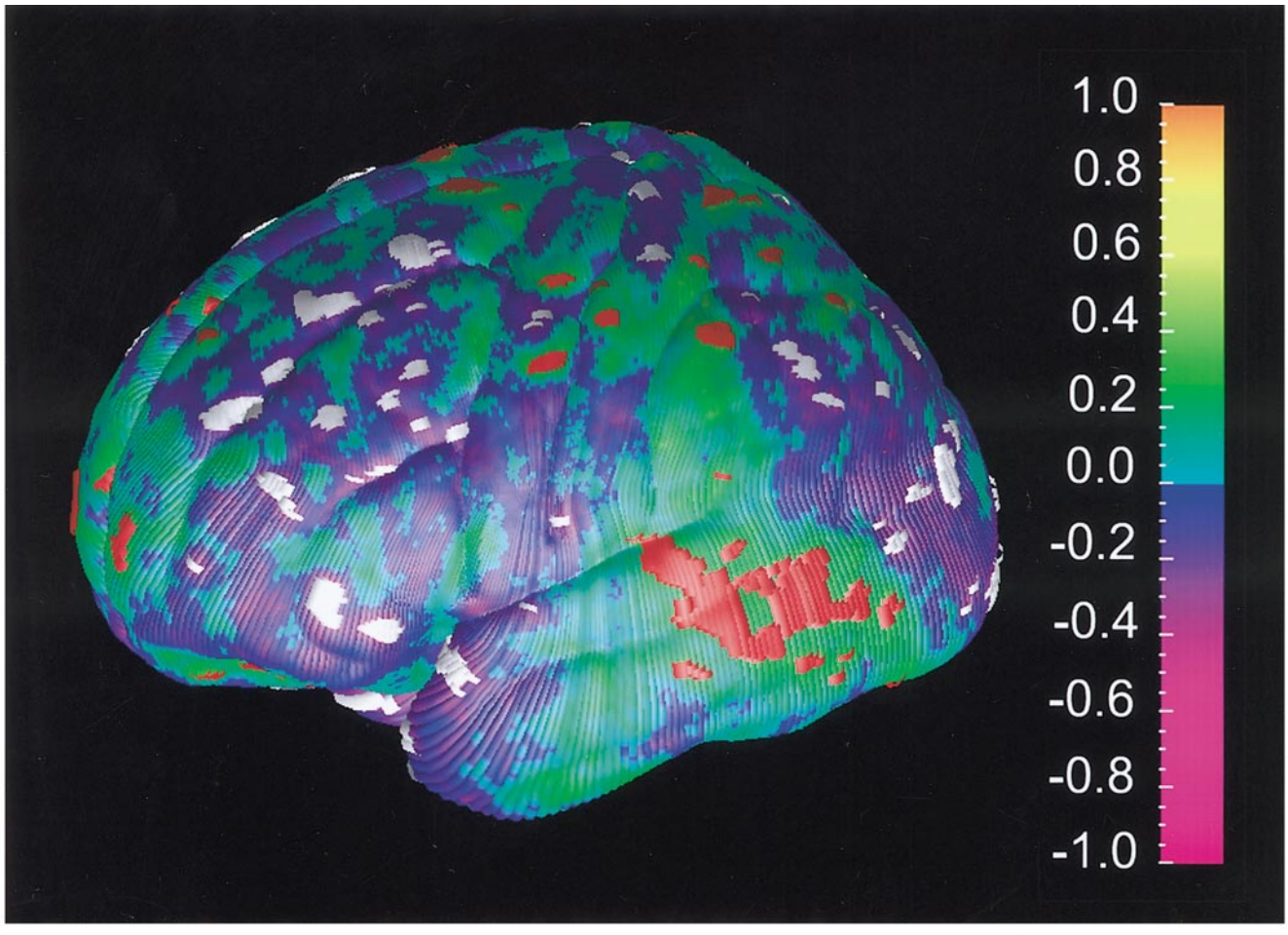

5

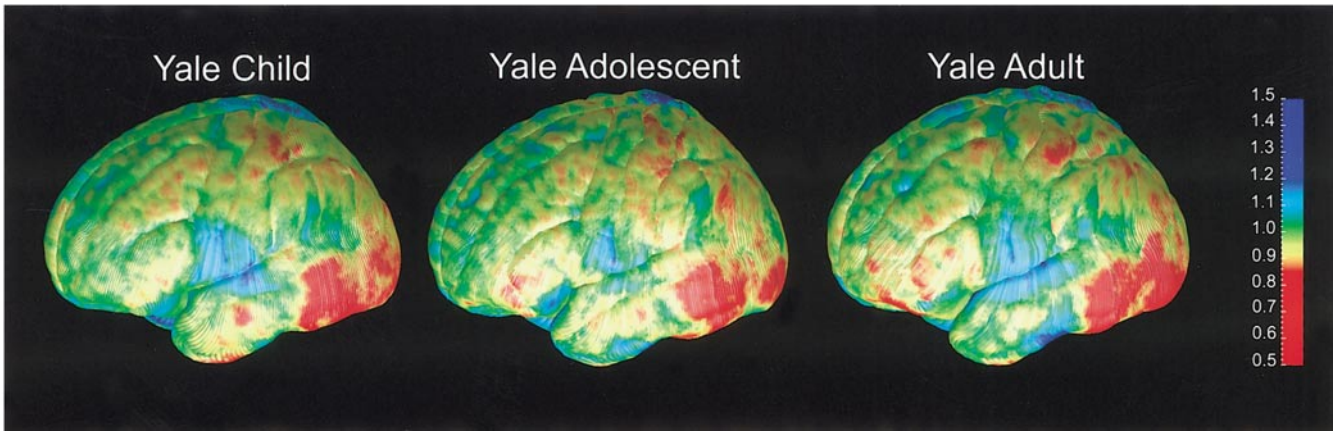

6

FIG. 5. Group difference in gray matter density asymmetry. A statistical map of the group difference (ALC vs SDC) in gray matter density asymmetry. Shades of green to yellow represent positive Pearson's correlation coefficients (regions where controls have more gray matter asymmetry than ALC) and shades of purple and pink represent negative Pearson's correlation coefficients (regions where ALC subjects have more asymmetry than the SDC subjects) according to the color bar on the right (range of Pearson correlation coefficients from -1 to $+1$). Regions shown in red correspond to correlation coefficients that show significant decrease in gray matter asymmetry in the ALC relative to SDC groups at a threshold of $P = 0.05$. Regions shown in white correspond to correlation coefficients that show significant increase in gray matter asymmetry in the ALC relative to SDC groups at a threshold of $P = 0.05$.

FIG. 6. Gray matter asymmetry maps for child, adolescent, and young adult groups. The color-coding for these maps is identical to that described for Fig. 5. Here we show gray matter density ratio maps for the 25 children (left), 15 adolescents (middle), and 16 young adults (right) in the YC group. The maps are virtually identical and statistical maps and permutation tests of the difference between child and adolescent and between adolescent and adult groups were not significant.

ter asymmetry. We then automatically transformed the ROIs from ICBM-305 average space back into the nonscaled, native image space of each individual subject (by inverting the transformation that took individuals from native to ICBM-305 space) and counted all voxels that segmented as gray matter and fell within the left or right hemisphere ROIs for each individual in native image space to obtain volume measures. An asymmetry ratio of the left to the right gray matter volume within the ROIs was calculated, and group differences in volume asymmetry were assessed with a Student *t* test. If differences between groups in gray matter *density* asymmetry reflect differences in *volume* asymmetry, we would expect this to be echoed in the *post hoc* volumetric analyses of differences in asymmetry between ALC and control subjects. The left and right ROIs from the group average in ICBM-305 space are shown mapped onto two individual subjects in native image space in Fig. 2.

RESULTS

Cortical Surface Asymmetry

Cortical surface asymmetry is shown mapped onto the average ALC brain surface, the average SDC brain surface, and the average YC brain surface, all in standard ICBM-305 space (Fig. 3). The arrows show the magnitude and direction of asymmetry at each brain surface point. Peak brain surface asymmetry is observed in all three groups in the peri-Sylvian region, where the distance between anatomically homologous surface points in the left and sulcally matched right brain surface is between 6 and 12 mm. Note that the direction of difference between the left and the right hemispheres cannot be described in simple "left greater than right" or "right greater than left" terms. This is because the displacement in homologous points between hemispheres embodies differences in the *x, y,* and *z* dimensions simultaneously as vectors (shown as arrows in Fig. 3). Given that the most robust asymmetry in the brain is in posterior perisylvian cortex, and given that the asymmetry is characterized by anterior–posterior displacement, we conducted statistical tests at each brain surface point to assess the significance of displacement between hemispheres at each point in only that direction. These statistical results are shown mapped on the ALC, SDC, and YC average brain surfaces in Fig. 3, and results from permutation tests assessing the statistical significance of the probability maps (while correcting for multiple comparisons) within frontal, temporal, parietal, and occipital regions for each group are shown in Table 2. The statistical maps and permutation results clearly show that anterior–posterior asymmetry, while most prominent in the peri-Sylvian region, is pervasive over vast regions of parietal, temporal, occipital, and some frontal cortices in all three groups. The permutation analyses show that surface asymmetry is overwhelmingly L > R (left more posterior than right), as shown by the arrows in Fig. 3 and in Table 2, in which the significance of results for the L > R (i.e., left more posterior than right) surface points far outweighs the significance of results for R > L surface points. The ALC–SDC group difference for *y*-coordinate asymmetry is significant in the occipital ROI. This effect is carried by the SDC group, having a significant L > R (right more posterior than left) hemispheric difference, which is lacking in the ALC group. The region of asymmetry in the occipital region of the SDC group lies on the undersurface of the brain (not shown in the figures). Notably, this effect is not significant in the YC group, which brings into question the robustness of the difference in ventral occipital asymmetry between ALC and control subjects.

Gray Matter Density Asymmetry

Gray matter density asymmetry maps for the ALC, SDC, and YC groups can be seen in Fig. 4. Note that the largest contiguous region of asymmetry is in the posterior inferior temporal lobe region in both SDC and YC groups. The region corresponds roughly to the intersection of Brodmann's areas 21, 22, and 37 (Brodmann, 1909). Gray matter density is greater in the right than in the left hemisphere in this region, and the statistical map of this effect is shown in Fig. 4. Right greater than left gray matter density asymmetry is also prominent in the occipital cortex, most notably in the YC group, but also seen in the ALC and SDC groups. The increased statistical power with the larger sample size in the YC group (i.e., $n = 62$ in the YC group vs 21 in the SDC group) results in smaller effects becoming statistically significant. Thus, the larger areas of statistically significant surface points shown in the statistical map of the YC group probably reflect the increased sample size. Results from permutation tests of differences in gray matter density between the left and the right hemispheres within frontal, temporal, parietal, and occipital regions for the ALC, SDC, and YC groups are shown in Table 3. The significance of right greater than left gray matter density is confirmed in occipital, parietal, and temporal lobes within both control groups. Left greater than right asymmetry is also significant in the temporal lobes in all three groups, as shown in the very anterior mesial regions of the temporal lobes shown in red in Fig. 4. Notably, the ALC group lacks significant right greater than left gray matter asymmetry in the temporal lobe, but the regional pattern of asymmetry is otherwise similar to the two control groups. A statistical map of the group difference (ALC vs SDC) in gray matter density asymmetry is shown in Fig. 5. Indeed, the apparent reduction in gray matter asymmetry in the ALC group is statistically significant within the posterior temporal lobes as shown in the statistical map and as confirmed with permutation ($P < 0.05$; see Table 3). Differences between groups (ALC vs SDC) in gray matter density asymmetry did not reach significance in any other region in the permutation analyses.

In Fig. 6, gray matter asymmetry maps are shown separately for the children in the YC group ($n = 26$, age 7 to 11), the adolescents in the YC group ($n = 15$, age 12 to 16), and the young adults in the YC group ($n = 16$, age 20 to 25). The maps look very similar and permutation tests of differences between the child and the adolescent and between the adolescent and the adult groups show no difference in gray matter density asymmetry in frontal, temporal, parietal, or occipital regions.

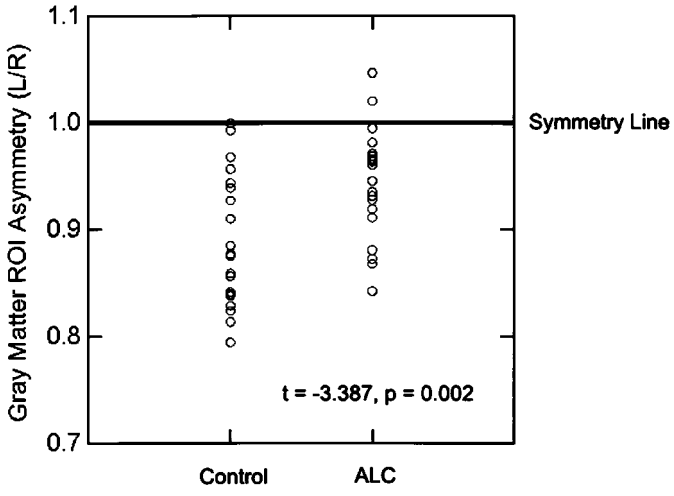

FIG. 7. Volume asymmetry graph. A ratio of the volume of gray matter in the left statistical region of interest (see Fig. 2) to the volume of gray matter in right statistical region of interest is plotted for the ALC and SDC groups. As shown, both groups show rightward asymmetry (i.e., numbers less than 1), but the SDC group has much more pronounced asymmetry in this region than the controls.

Post Hoc Volumetric Asymmetry Analyses

In the ALC and SDC groups, we counted the number of voxels in the left hemisphere which segmented as gray matter and fell within the region of interest derived from the statistical map of hemispheric difference in gray matter density in the SDC group (see Fig. 2). We also counted the number of voxels within the same region of interest flipped into the right hemisphere, and then created a ratio (L/R) of these measures to assess volumetric gray matter asymmetry. The results from these analyses are shown in graphic format in Fig. 7. While both ALC and SDC groups show a rightward gray matter volume asymmetry in the posterior temporal lobes, the degree of asymmetry is significantly greater in the SDC group ($t = -3.387$, $P = 0.002$), further confirming results shown in the statistical maps.

DISCUSSION

To our knowledge, this is the first report in the literature of brain surface and gray matter density asymmetry patterns in normally developing children and adolescents and in individuals with severe prenatal alcohol exposure. Here we show that gray matter asymmetry within the posterior inferior temporal lobes is altered in the alcohol-exposed subjects. These individuals showed reduced rightward asymmetry in this region, whether assessed with surface-based or volumetric image analysis methods. This result is consistent with our earlier findings in these subjects in which gray matter density was more affected in the left hemisphere than in the right (Sowell *et al.*, 2001b, 2002a). The region of altered asymmetry is primarily at the conjunction of Brodmann's areas 21, 22, and 37 (Brodmann, 1909). Functional imaging studies have shown that areas 21 and 22 are primarily involved in language processing, while area 37 is involved with object and face recognition (reviewed in Cabeza and Nyberg, 2000). Cognitive functions subserved by these regions have been shown to be deficient in individuals with severe prenatal alcohol exposure (Church and Abel, 1998; Mattson *et al.*, 1998). Perhaps the altered gray matter asymmetry in the ALC subjects contributes to these specific cognitive deficits.

In this report, cortical gray matter density asymmetry patterns have been mapped in normal children, adolescents, and young adults using anatomical landmarks to match cortical anatomy across subjects. Here we show that the most prominent gray matter asymmetry at the brain surface is in the posterior temporal lobes, whether looking at children, adolescents, or young adults. This finding was confirmed in two independent samples of normal control subjects scanned on different scanners by different research groups, further establishing the validity of our results. Age effects in gray matter asymmetry between the normal child and adolescent groups and between the normal adolescent and young adult groups were not significant, suggesting that the pattern of gray matter asymmetry is established early in development. Right greater than left gray matter asymmetry in the posterior, superior temporal sulcus has previously been reported in a large imaging study of young adults (Watkins *et al.*, 2001). White matter asymmetry in this region has also been examined with MRI, and results have shown left greater than right white matter asymmetry in the primary auditory cortex (Penhune *et al.*, 1996), a region proximal to that observed here. Left greater than right white matter asymmetry in the posterior temporal lobes has been reported in the postmortem literature as well (Anderson *et al.*, 1999). While we measured the proportion of voxels that segmented as *gray* matter within a 15-mm sphere attached to each brain surface point, it is possible that we measured less gray matter in the left hemisphere because there was actually more white matter present with an opposite pattern in the right hemisphere. Thus, the white matter asymmetry findings from postmortem and *in vivo* samples may be consistent with the gray matter results reported here and by other research groups (Watkins *et al.*, 2001).

Analyses of brain surface asymmetry revealed prominent effects in the peri-Sylvian region in the control subjects, and this asymmetry did not differ in the ALC group. This asymmetry is characterized by posterior displacement of the left posterior temporal and inferior parietal cortex relative to the right, a finding that has been reported in numerous other studies (Galaburda *et al.*, 1978; Ide *et al.*, 1996; Narr *et al.*, 2001; Sowell *et al.*, 2002b; Thompson *et al.*, 1998). Here we have mapped asymmetry over the entire brain surface. The resulting vector maps show that the direction of displacement between hemispheres in all brain regions is primarily in the anterior–posterior axis and arises primarily from the left being more posterior than right.

The ALC group differed from the SDC group on measures of anterior–posterior asymmetry in permutation analyses, but this group difference was not expected. It occurred in a region on the ventral surface of the occipital lobe that does not show prominent asymmetry (in terms of millimeters of difference between hemispheres) in any group studied. The two control groups were discrepant in this region as well,

with the SDC group showing significant asymmetry and the YC group not showing significant asymmetry in the permutation analyses, adding to our hesitation to interpret this result. Further studies will be needed to examine possible anterior–posterior asymmetry on the ventral surface of the occipital lobes and its alteration in individuals with prenatal alcohol exposure.

Our results of gray matter asymmetry in normal individuals are only partially consistent with the results described in two recent reports (Good *et al.*, 2001; Watkins *et al.*, 2001) which have documented cerebral asymmetry in brain gray and white matter using whole-brain voxel-based morphometry. In these studies, brain image gray matter data sets in large samples of normal adults were automatically scaled into standard space and statistically compared, on a voxel-by-voxel basis, to the mirror images of the same brain data sets after they had been flipped around the parasagittal plane. In both studies (Good *et al.*, 2001; Watkins *et al.*, 2001), the most prominent finding was an increase in gray matter in the right frontal lobe compared to the left and an increase in gray matter in the left occipital lobe compared to the right. These findings mark the most robust gross structural asymmetry in the brain known as the left frontal and right occipital petalias. Essentially, the frontal and occipital lobes lie in different locations in each hemisphere, with the frontal lobe extending farther anteriorly in the right hemisphere and the occipital lobe extending farther posteriorly in the left hemisphere (Weinberger *et al.*, 1982). We did not observe this pattern of asymmetry in our analyses, probably because we manually matched cortical anatomy between the hemispheres before assessing gray matter density hemispheric differences.

Some caveat is warranted when interpreting gray matter asymmetry patterns given the prominent spatially dependent nonuniformity of voxel intensities frequently found in MRI data (DeCarli *et al.*, 1996). We have observed that the pattern of nonuniformity tends to run diagonally across the brain, at least on the magnet used to image all of the subjects studied here (i.e., Signa; General Electric). The right frontal lobes tend to have lower signal than the left, and the left occipital lobes tend to have a lower signal value than the right. This effect is not completely eliminated with the inhomogeneity intensity correction algorithm used here (Sled *et al.*, 1998) and also used by Watkins and colleagues in their study of gray matter asymmetry (Watkins *et al.*, 2001). Thus, it is possible that the gray matter asymmetry pattern observed by us, and by others before us, is not about morphological differences between the hemispheres but about differences in voxel intensity due to inhomogeneity artifact. However, the findings of white matter asymmetry in the posterior temporal lobes in postmortem data, not subject to scanner artifact, suggest that our observations are valid. Also, the ALC and control subjects (SDC and YC) were scanned in the same type of magnet, with presumably the same artifact, so the effect of inhomogeneity would be subtracted out in group difference analyses. Given this, we are confident about the altered gray matter asymmetry pattern reported here in the alcohol-exposed subjects, but issue more caution in interpreting the gray matter asymmetry maps within groups.

While we attribute the morphological abnormalities in the ALC subjects to the prenatal alcohol exposure, it is possible that other environmental factors (pre- or postnatal) unique to the ALC group could also result in the aberrant asymmetry. For example, many of the mothers of ALC subjects studied here also smoked during pregnancy, but defining features characteristic of individuals with fetal alcohol syndrome are not found in children of mothers who smoked but did not drink heavily during pregnancy (e.g., Ernst *et al.*, 2001). Other drugs may have been used by the mothers of the ALC subjects as well, but they were characterized as "alcohol dependent" and not "drug dependent" by medical, legal, and family reports. Nutritional differences during pregnancy could also be a factor in the brain dysmorphology observed, but animal studies have shown brain growth restriction in animals with neonatal alcohol exposure when nutritional intake was well controlled (e.g., Byrnes *et al.*, 2001). Nonetheless, environmental teratogens other than alcohol cannot be completely ruled out as contributing factors to brain dysmorphology in this human sample.

ACKNOWLEDGMENTS

Funding for this work was provided by NIMH K01 MH01733 (E.R.S.); NCRR P41 RR13642, NINDS NS3753 (A.W.T.); NIAAA AA 10417 (E.P.R.), AA 10820 (S.N.M.), MH01232 (B.S.P.), and MH59239 (B.S.P.).

REFERENCES

Anderson, B., Southern, B. D., and Powers, R. E. 1999. Anatomic asymmetries of the posterior superior temporal lobes: A postmortem study. *Neuropsychiatry Neuropsychol. Behav. Neurol.* **12:** 247–254.

Archibald, S. L., Fennema-Notestine, C., Gamst, A., Riley, E. P., Mattson, S. N., and Jernigan, T. L. 2001. Brain dysmorphology in individuals with severe prenatal alcohol exposure. *Dev. Med. Child. Neurol.* **43:** 148–154.

Blanton, R. E., Levitt, J. G., Thompson, P. M., Narr, K. L., Capetillo-Cunliffe, L., Nobel, A., Singerman, J. D., McCracken, J. T., and Toga, A. W. 2001. Mapping cortical asymmetry and complexity patterns in normal children. *Psychiatry Res.* **107:** 29–43.

Bookstein, F. L., Sampson, P. D., Streissguth, A. P., and Connor, P. D. 2001. Geometric morphometrics of corpus callosum and subcortical structures in the fetal-alcohol-affected brain. *Teratology* **64:** 4–32.

Brodmann, K. 1909. *Vergleichende Lokalisationlehre Der Grosshimrinde in ihren' Prinzipien dargestellt auf Grund in Zellenbaues.* Barth, Leipzig.

Byrnes, M. L., Reynolds, J. N., and Brien, J. F. 2001. Effect of prenatal ethanol exposure during the brain growth spurt of the guinea pig. *Neurotoxicol. Teratol.* **23:** 355–364.

Cabeza, R., and Nyberg, L. 2000. Imaging cognition. II. An empirical review of 275 PET and fMRI studies. *J. Cognit. Neurosci.* **12:** 1–47.

Church, M. W., and Abel, E. L. 1998. Fetal alcohol syndrome: Hearing, speech, language, and vestibular disorders. *Obstet. Gynecol. Clin. North Am.* **25:** 85–97.

DeCarli, C., Murphy, D. G., Teichberg, D., Campbell, G., and Sobering, G. S. 1996. Local histogram correction of MRI spatially depen-

dent image pixel intensity nonuniformity. *J. Magn. Reson. Imaging* **6:** 519–528.

Duvernoy, H. M., Cabanis, E. A., and Vannson, J. L. 1991. *The Human Brain: Surface, Three-Dimensional Sectional Anatomy and MRI.* Springer-Verlag, Vienna/New York.

Ernst, M., Moolchan, E. T., and Robinson, M. L. 2001. Behavioral and neural consequences of prenatal exposure to nicotine. *J. Am. Acad. Child. Adolesc. Psychiatry* **40:** 630–641.

Evans, A. C., Collins, D. L., and Holmes, C. J. 1996. *Automatic 3D Regional MRI Segmentation and Statistical Probabilistic Anatomical Maps.* Academic Press, New York.

Galaburda, A. M., Sanides, F., and Geschwind, N. 1978. Human brain: Cytoarchitectonic left–right asymmetries in the temporal speech region. *Arch. Neurol.* **35:** 812–817.

Geschwind, N., and Levitsky, W. 1968. Human brain: Left–right asymmetries in temporal speech region. *Science* **161:** 186–187.

Good, C. D., Johnsrude, I., Ashburner, J., Henson, R. N., Friston, K. J., and Frackowiak, R. S. 2001. Cerebral asymmetry and the effects of sex and handedness on brain structure: A voxel-based morphometric analysis of 465 normal adult human brains. *NeuroImage* **14:** 685–700.

Habib, M., Robichon, F., Levrier, O., Khalil, R., and Salamon, G. 1995. Diverging asymmetries of temporo-parietal cortical areas: A reappraisal of Geschwind/Galaburda theory. *Brain Lang.* **48:** 238–258.

Ide, A., Rodriguez, E., Zaidel, E., and Aboitiz, F. 1996. Bifurcation patterns in the human sylvian fissure: Hemispheric and sex differences. *Cereb. Cortex* **6:** 717–725.

Jones, K. L., and Smith, D. W. 1973. Recognition of the fetal alcohol syndrome in early infancy. *Lancet* **2:** 999–1001.

Jones, K. L., and Smith, D. W. 1975. The fetal alcohol syndrome. *Teratology* **12:** 1–10.

Kulynych, J. J., Vladar, K., Jones, D. W., and Weinberger, D. R. 1994. Gender differences in the normal lateralization of the supratemporal cortex: MRI surface-rendering morphometry of Heschl's gyrus and the planum temporale. *Cereb. Cortex* **4:** 107–118.

LeMay, M., and Culebras, A. 1972. Human brain—Morphologic differences in the hemispheres demonstrable by carotid arteriography. *N. Engl. J. Med.* **287:** 168–170.

MacDonald, D., Avis, D., and Evans, A. 1994. Multiple surface identification and matching in magnetic resonance images. *Proc. Visualizat. Biomed. Comput.* **2359,** 160–169.

Mattson, S. N., Goodman, A. M., Caine, C., Delis, D. C., and Riley, E. P. 1999. Executive functioning in children with heavy prenatal alcohol exposure. *Alcohol. Clin. Exp. Res.* **23:** 1808–1815.

Mattson, S. N., and Riley, E. P. 1999. Implicit and explicit memory functioning in children with heavy prenatal alcohol exposure. *J. Int. Neuropsychol. Soc.* **5:** 462–471.

Mattson, S. N., Riley, E. P., Delis, D. C., Stern, C., and Jones, K. L. 1996a. Verbal learning and memory in children with fetal alcohol syndrome. *Alcohol. Clin. Exp. Res.* **20:** 810–816.

Mattson, S. N., Riley, E. P., Gramling, L., Delis, D. C., and Jones, K. L. 1998. Neuropsychological comparison of alcohol-exposed children with or without physical features of fetal alcohol syndrome. *Neuropsychology* **12:** 146–153.

Mattson, S. N., Riley, E. P., Sowell, E. R., Jernigan, T. L., Sobel, D. F., and Jones, K. L. 1996b. A decrease in the size of the basal ganglia in children with fetal alcohol syndrome. *Alcohol. Clin. Exp. Res.* **20:** 1088–1093.

Mazziotta, J. C., Toga, A. W., Evans, A., Fox, P., and Lancaster, J. 1995. A probabilistic atlas of the human brain: Theory and rationale for its development. The International Consortium for Brain Mapping. *NeuroImage* **2:** 89–101.

Narr, K. L., Thompson, P. M., Sharma, T., Moussai, J., Zoumalan, C., Rayman, J., and Toga, A. W. 2001. Three-dimensional mapping of gyral shape and cortical surface asymmetries in schizophrenia: Gender effects. *Am. J. Psychiatry* **158:** 244–255.

Ono, M., Kubik, S., and Abernathey, C. D. 1990. *Atlas of the Cerebral Sulci.* Thieme, Stuttgart/New York.

Penhune, V. B., Zatorre, R. J., MacDonald, J. D., and Evans, A. C. 1996. Interhemispheric anatomical differences in human primary auditory cortex: Probabilistic mapping and volume measurement from magnetic resonance scans. *Cereb. Cortex* **6:** 661–672.

Peterson, B. S., Staib, L., Scahill, L., Zhang, H., Anderson, C., Leckman, J. F., Cohen, D. J., Gore, J. C., Albert, J., and Webster, R. 2001. Regional brain and ventricular volumes in Tourette syndrome. *Arch. Gen. Psychiatry* **58:** 427–440.

Roebuck, T. M., Mattson, S. N., and Riley, E. P. 1998. A review of the neuroanatomical findings in children with fetal alcohol syndrome or prenatal exposure to alcohol. *Alcohol. Clin. Exp. Res.* **22:** 339–344.

Sled, J. G., Zijdenbos, A. P., and Evans, A. C. 1998. A nonparametric method for automatic correction of intensity nonuniformity in MRI data. *IEEE Trans. Med. Imaging* **17:** 87–97.

Sowell, E. R., Mattson, S. N., Thompson, P. M., Jernigan, T. L., Riley, E. P., and Toga, A. W. 2001a. Mapping callosal morphology and cognitive correlates: Effects of heavy prenatal alcohol exposure. *Neurology* **57:** 235–244.

Sowell, E. R., Thompson, P. M., Holmes, C. J., Batth, R., Jernigan, T. L., and Toga, A. W. 1999. Localizing age-related changes in brain structure between childhood and adolescence using statistical parametric mapping. *NeuroImage* **9:** 587–597.

Sowell, E. R., Thompson, P. M., Mattson, S. N., Tessner, K. D., Jernigan, T. L., Riley, E. P., and Toga, A. W. 2001b. Voxel-based morphometric analyses of the brain in children and adolescents prenatally exposed to alcohol. *NeuroReport* **12:** 515–523.

Sowell, E. R., Thompson, P. M., Mattson, S. N., Tessner, K. D., Jernigan, T. L., Riley, E. P., and Toga, A. W. 2002a. Regional brain shape abnormalities persist into adolescence after heavy prenatal alcohol exposure. *Cereb. Cortex* **12**(8): 856–865.

Sowell, E. R., Thompson, P. M., Rex, D., Kornsand, D., Jernigan, T. L., and Toga, A. W. 2002b. Mapping sulcal pattern asymmetry and local cortical surface gray matter proportion in vivo: Maturation in posterior perisylvian cortices. *Cereb. Cortex* **12:** 17–26.

Sowell, E. R., Thompson, P. M., Tessner, K. D., and Toga, A. W. 2001c. Mapping continued brain growth and cortical gray matter density reduction in frontal cortex: Inverse relationships during post adolescent brain maturation. *J. Neurosci.* **21:** 8819–8829.

Steinmetz, H., Herzog, A., Schlaug, G., Huang, Y., and Jancke, L. 1995. Brain (A)symmetry in monozygotic twins. *Cereb. Cortex* **5:** 296–300.

Steinmetz, H., Volkmann, J., Jancke, L., and Freund, H. J. 1991. Anatomical left–right asymmetry of language-related temporal cortex is different in left- and right-handers. *Ann. Neurol.* **29:** 315–319.

Swayze, V. W., Johnson, V. P., Hanson, J. W., Piven, J., Sato, Y., Giedd, J. N., Mosnik, D., and Andreasen, N. C. 1997. Magnetic resonance imaging of brain anomalies in fetal alcohol syndrome. *Pediatrics* **99:** 232–240.

Thompson, P. M., Mega, M. S., Woods, R. P., Zoumalan, C. I., Lindshield, C. J., Blanton, R. E., Moussai, J., Holmes, C. J., Cummings, J. L., and Toga, A. W. 2001. Cortical change in Alzheimer's disease detected with a disease-specific population-based brain atlas. *Cereb. Cortex* **11:** 1–16.

Thompson, P. M., Moussai, J., Zohoori, S., Goldkorn, A., Khan, A. A., Mega, M. S., Small, G. W., Cummings, J. L., and Toga, A. W. 1998.

Cortical variability and asymmetry in normal aging and Alzheimer's disease. *Cereb. Cortex* **8:** 492–509.

Thompson, P. M., Woods, R. P., Mega, M. S., and Toga, A. W. 2000. Mathematical/computational challenges in creating deformable and probabilistic atlases of the human brain. *Hum. Brain Mapping* **9:** 81–92.

Wada, J. A., Clarke, R., and Hamm, A. 1975. Cerebral hemispheric asymmetry in humans: Cortical speech zones in 100 adults and 100 infant brains. *Arch. Neurol.* **32:** 239–246.

Watkins, K. E., Paus, T., Lerch, J. P., Zijdenbos, A., Collins, D. L., Neelin, P., Taylor, J., Worsley, K. J., and Evans, A. C. 2001. Structural asymmetries in the human brain: A voxel-based statistical analysis of 142 MRI scans. *Cereb. Cortex* **11:** 868–877.

Weinberger, D. R., Luchins, D. J., Morihisa, J., and Wyatt, R. J. 1982. Asymmetrical volumes of the right and left frontal and occipital regions of the human brain. *Ann. Neurol.* **11:** 97–100.

Witelson, S. F., and Pallie, W. 1973. Left hemisphere specialization for language in the newborn. Neuroanatomical evidence of asymmetry. *Brain* **96:** 641–646.

Woods, R. P., Mazziotta, J. C., and Cherry, S. R. 1993. MRI–PET registration with automated algorithm. *J. Comput. Assisted Tomogr.* **17:** 536–546.